DOI: 10.13009/EUCASS2017-147

Diffuse interface modelling for the primary atomization in cryogenic rocket engines

Aymeric Boucher and Angelo Murrone**
** ONERA - The French Aerospace Lab*
F-92322 Châtillon, France

Abstract

In this paper, we propose diffuse interface models for the simulation of separated two-phase flow in cryogenic injector. Instead of using a 4 equation model [40], we intend to improve velocity and temperature description of the phases with 7 and 5 equation models. Then, we focus on the numerical resolution. For the 7 equation, we apply the simple HLLC scheme [23] combined with a MUSCL technique [35]. For the 5 equation, we derive HLLC type schemes based on different system's formulations. Finally, we present the numerical results obtained on validation test cases and on a coaxial injector configuration.

1. Introduction

To help the development and enhancement of launcher propulsion systems and to ensure their reliability, we have to study in a more comprehensive way all physical process involved in the combustion chamber. For liquid rocket engines, this is a major issue which concerns a large variety of multi-scale phenomena such as combustion, cavitation, evaporation, turbulence and atomization. Moreover, the complex interaction between propellants injection, flame dynamics and acoustic modes can generate high frequency instabilities which can cause highly destructive damages. In this study, we suggest to focus on injection which plays a key role to controlled combustion under transient operating conditions. Indeed, the physical processes in the chamber are highly dependent on the characteristics of the spray produced.

The Figure 1 represents the different phenomena in a coaxial cryogenic injector in subcritical conditions. Initial breakup of the bulk liquid namely the primary atomization occurs near the injector. The formation into child droplets namely the secondary atomization occurs downstream. Following the classification of Ishii [28], this two-phase flow infers a dense "separated" liquid phase near the injector as well as a "dispersed" liquid phase. In the dense region of the liquid jet, the atomization results from interaction between liquid LOx and gaseous H_2 phases. The dispersion process is due to the strong difference of velocity between the two phases. Ligaments start growing from the liquid core because of Kelvin-Helmholtz and Rayleigh-Taylor interfacial instabilities. These ligaments thus formed are unstable and undergo breakup producing droplets when disruptive forces exceed the liquid surface tension and viscous forces. This results in a spray of smaller oxygen droplets with final stable sizes, mainly spherical, which are dispersed by the turbulent gas flow, and finally vaporized to feed the combustion with hydrogen H_2. The gas phase is made up with hydrogen H_2, vaporized oxygen O_2, and combustion products. Eventually, the resulting hot and high-pressure combustion products exhaust through a nozzle at supersonic speed, thereby providing the required thrust.

A lot of experimental and theoretical are addressed for this problem but this breakup cascade remains an actual debate. There are no sufficient results to provide parameters like the expansion angle, the penetration depth, the droplet size distribution. The main reason is the droplets cloud surrounding the liquid core region and blocking access to optical rays. Moreover, it is difficult to view phenomena because the length and time characteristics are very small. Nevertheless, with recent improvements in optical ray and x-ray imaging techniques, a detailed analysis [42] of gas liquid interface has been provided. For the MASCOTTE cryogenic injector [57], the spray was recently investigated with a high speed camera in a backlighting optical configuration [38]. On the other hand, experiments concerning diesel injection are gaining importance [59], [14], [44]. We expect that in a near future, spatial resolution at the sub-micro-meter level may provide data base for cryogenic rocket engine but also for Direct Injection Diesel.

DOI: 10.13009/EUCASS2017-147

Concerning numerical simulation, computational resources give us the possibility to view the atomization process more accurately than before and DNS are gaining importance [22], [19], [25], [26]. A lot of works are based on the ARCHER software [41] which combines a level set with a VOF method. In [21], DNS of two-phase flow provides very promising results. Nevertheless, the finest scales of two-phase flow are not known contrary to Kolmogorov scale and cannot be resolved even if the mesh size is the order of 0.35µm. Other recent works of DNS can also be mentioned [8] but it seems that DNS is not enough mature for industrial configurations. In fact, the simulation required in liquid propulsion as depicted in Figure 1, even only applied to one single coaxial cryogenic injector, remains a tremendous challenge when considering atomization of the jet combined with the combustion of the spray.

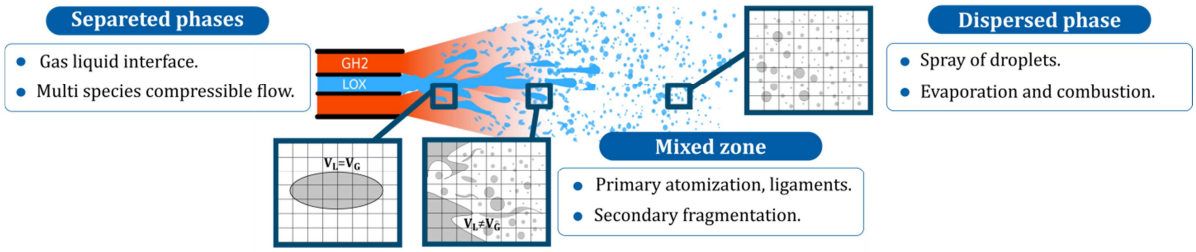

Figure 1: schematic representation of a coaxial cryogenic injector

So, a lot of numerical works are based on RANS and LES approach when we consider the modelling of primary atomization in cryogenic rocket engines or in Direct Injection Diesel. These approaches need sub-grid models which can be derived from theoretical, experimental or DNS results [21]. Concerning cryogenic combustion the work of [52], [55], [56] initially started for Diesel engines are very interesting. A 4 equation diffuse interface model is combined with a sophisticated surface density equation which is a mandatory as explained in [37]. This last equation contains source terms for creation and destruction of interface area which are closed with turbulent RANS approach. The basis of the model has been used in [45], [36] and applied to a coaxial injector in [16]. Then new closure of the source terms are suggested in [29], [30]. The recent work of [17] deals with the liquid jet atomization under direct diesel engine conditions but combustion is not accounted for. A 7 equation diffuse interface model [10] with procedures relaxation of pressure, velocity [48] and temperature [60] is used both for the liquid core and the spray droplets. A new atomization model is formulated using two surface density equations. The closure terms are based on RANS simulation and the turbulence is necessary for liquid and gas. They highlight that a unique surface density equation is used in [54], [32] for the two phases. Here, two surface density equations are transported with the same interface velocity; one for the dense “separated” phases and another one for the “dispersed” phase. The objective is to improve atomization but also breakup modelling. In [1], a QME quasi multiphase Eulerian solver is implemented in OpenFOAM and applied to a jet in crossflow. Comparison with experiments and DNS [25], [26] are presented. The innovative second order closure for the slip velocity is based on transport equations for momentum, volume fraction, surface density and liquid flux. It means a gap between fully multiphase and mixture approach since it holds for a large range of liquid volume fraction going from dense “separated” to “dispersed” flow. Concerning Diesel Injection, a new model is proposed in [5] and combines the 4 equation RANS approach with a Lagrangian description for the spray into the ELSA (Eulerian Lagrangian Spray Atomization) code. Following this strategy, works of [32] make the source terms depending on “dispersed” or “separated” topology of the two-phase flows and they improve the definition of the equilibrium Weber number. The strategy is continuing in the RANS context with [31] but it seems that the strong coupling between Eulerian and Lagrangian methods induces some difficulties [20]. In [25], an efficient parallel multi-scale coupling procedure between an Eulerian level set method tracking interface and a standard Lagrangian description of small scales has been applied successfully to a turbulent liquid jet under Diesel engine conditions. Then works [11], [12], [13] focus on interfacial area equation in the LES context and use also accurate tracking interface methods.

In the Eulerian-Lagrangian methods sometimes associated with a tracking interface method, several difficulties arise. The first one is due to the lack of robustness of the Lagrangian methods in the case of strong two-way coupling. The second one is related to the statistical interpretation of numerous numerical particles produced in the atomization area. It seems also that taking into account for the compressibility of the fluid with the tracking interface method is not an easy task.
In the Eulerian-Eulerian methods, the principal drawback is the numerical diffusion of the interfaces. One major advantage against interface tracking and Lagrangian methods is that models are general and fully compressible. A second one is that Eulerian-Eulerian methods are also well adapted to parallel and time implicit computations.

DOI: 10.13009/EUCASS2017-147

In a previous works [40], we have proposed a coupling strategy between a 4 equation diffuse interface model and an Eulerian kinetic model for the spray. The fully Eulerian coupling between “separated” and “dispersed” two-phase flow solvers has been implemented in the ONERA's CEDRE code [43] and has been applied to the simulation of the MASCOTTE [24], [57], [53], [38] test facility on the 10-bar operating point corresponding to cryogenic rocket engines under transient operating conditions as depicted in Figure 2.

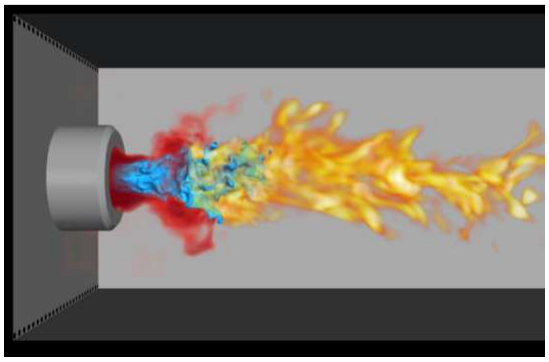

Figure 2: LES of a subcritical combustion LOx/GH2 (10-bar operating MASCOTTE 10 facility)
(Liquid oxygen in blue, hydrogen in red and flame in yellow)

In this paper, we focus on diffuse interface models for the simulation of separated two-phase flow in coaxial cryogenic injector in order to realize in the future the same coupling strategy than before and to derive a new model for atomization. Actually, we propose an improvement of the diffuse interface model to deal with the separated two-phase flow near the injector for the liquid core. Instead of using the 4 equation model, we have selected the 7 (two pressures, two velocities and two temperatures) and the 5 (two temperatures) equation models. The two momentum transported by the 7 equation model [10] should give us a better description of the liquid velocity in the diffuse interface where a large difference between liquid and gas velocities exists. The two temperatures of the 5 equation model [39] provide an accurate description of the liquid temperature and should be able to avoid spurious pressure oscillations of the 4 equation model due to mixing of hot gas with cold liquid in the diffuse interface. These two models and the derivation of the 5 equation model are presented in the next section 2. Then section 3 is devoted to build accurate and robust schemes for simulations including large difference of velocity and high density ratio between the two phases. For the 7 equation, we apply the simple HLLC scheme [23] combined [6] with a MUSCL technique [35]. For the 5 equation, we derive HLLC type schemes [7] based on different system’s formulations to get the more robust scheme as possible. Finally in section 4, we present the numerical results obtained on validation test cases and on a coaxial injector configuration.

2. Governing equations

In the framework of diffuse interface modelling which we have selected to deal with separated two-phase flows, different level of description are available. Modelling of two-phase flows is typically based on averaging procedures [28], [18]. In their most general form, these averaging techniques produce models characterized by two different velocities and pressures for each phase supplemented by one or several topological equations. This is namely the 7 equation model [10], [48]. On the opposite, a very simple 4 equation bi-species Navier-Stokes system as in [40] can also be employed. As usual, a delicate balance between the complexity of the model and its performance has to be found. In the dense region of the two-phase flow, we propose to use a more sophisticated interface diffuse model than previously. In this context, the 7 and 5 equation model have been selected in this paper. The 7 equation model allows us to describe the interface between gas-liquid with two different velocities and temperatures while the 5 equation provides only two different temperatures. Besides, we point out that works dealing with liquid gas interface simulations and diffuse interface modelling are gaining importance [49], [34].

2.1 The seven equation model

If we extend this 7 equation model to the case of multi-species fluid, mass conservation equation may be readily replaced by mass fractions equations and the convective part of the $(5+n_1+n_2)$ equations system with relaxation pressures, velocities and temperatures source terms can be written under the form:

DOI: 10.13009/EUCASS2017-147

$$\frac{\partial(\alpha_1\rho_1 Y_1^i)}{\partial t} + div(\alpha_1\rho_1 Y_1^i \boldsymbol{u}_1) = w_1^i$$
$$\frac{\partial(\alpha_1\rho_1\boldsymbol{u}_1)}{\partial t} + div(\alpha_1\rho_1\boldsymbol{u}_1\otimes\boldsymbol{u}_1) + \nabla(\alpha_1 p_1) = p_I\nabla\alpha_1 + \lambda(\boldsymbol{u}_2 - \boldsymbol{u}_1) + \boldsymbol{u_I}m$$
$$\frac{\partial(\alpha_1\rho_1 e_1)}{\partial t} + div(\alpha_1(\rho_1 e_1 + p_1)\boldsymbol{u}_1) = p_I\boldsymbol{u_I}\cdot\nabla\alpha_1 + \lambda\boldsymbol{u_I}\cdot(\boldsymbol{u}_2 - \boldsymbol{u}_1) + p_I\mu(p_2 - p_1) + Q + \left(e_I + \frac{\boldsymbol{u_I}^2}{2}\right)m$$
$$\frac{\partial(\alpha_2\rho_2 Y_2^i)}{\partial t} + div(\alpha_2\rho_2 Y_2^i \boldsymbol{u}_2) = w_2^i$$
$$\frac{\partial(\alpha_2\rho_2\boldsymbol{u}_2)}{\partial t} + div(\alpha_2\rho_2\boldsymbol{u}_2\otimes\boldsymbol{u}_2) + \nabla(\alpha_2 p_2) = -p_I\nabla\alpha_1 - \lambda(\boldsymbol{u}_2 - \boldsymbol{u}_1) - \boldsymbol{u_I}m$$
$$\frac{\partial(\alpha_2\rho_2 e_2)}{\partial t} + div(\alpha_2(\rho_2 e_2 + p_2)\boldsymbol{u}_2) = -p_I\boldsymbol{u_I}\cdot\nabla\alpha_1 - \lambda\boldsymbol{u_I}\cdot(\boldsymbol{u}_2 - \boldsymbol{u}_1) - p_I\mu(p_2 - p_1) - Q - \left(e_I + \frac{\boldsymbol{u_I}^2}{2}\right)m$$
$$\frac{\partial\alpha_k}{\partial t} + \boldsymbol{u_I}\cdot\nabla\alpha_k = -\mu(p_{k'} - p_k) + \frac{Q}{\kappa} + \frac{m}{\varrho} \quad (1)$$

The notations are classical. Firstly, α_k are the volume fractions of each phase ($\alpha_1 + \alpha_2 = 1$), ρ_k the phase densities, $\boldsymbol{u}_k$ the vector velocities, p_k the pressures and $e_k = \varepsilon_k + \boldsymbol{u}_k^2/2$ the specific total energies, with ε_k the specific internal energies. On the other hand, $\boldsymbol{u_I}, p_I$ stand for the interfacial velocity and pressure:

$$\boldsymbol{u_I} = \sum_{k=1}^{2}\alpha_k\rho_k\boldsymbol{u}_k \Big/ \sum_{k=1}^{2}\alpha_k\rho_k\,, \qquad p_I = \sum_{k=1}^{2}\alpha_k p_k \quad (2)$$

The model contains mechanical effects for the pressure and velocity relaxations. Moreover the two terms Q, m stand respectively for the heat and mass transfer and can be written under the form:

$$Q = \theta(T_2 - T_1), \qquad m = \nu(g_2 - g_1) \quad (3)$$

The convective part of the system can be written under the following form:

$$\frac{\partial Q_k}{\partial t} + div\big(G(Q_k)\big) = H_k\cdot\nabla\alpha_k + R_k \quad (4)$$

For each phase k, the vector Q_k stands for the conservative variables, $G(Q_k)$ for the flux vector while $H_k\cdot\nabla\alpha_k$ denotes the non-conservative part of the system. In the other hand, R_k are respectively the relaxation terms for pressures, velocities, temperatures and free energies. The terms of the convective part of the system write:

$$Q_k = \begin{bmatrix}\alpha_k\rho_k Y_k^i\\ \alpha_k\rho_k\boldsymbol{u}_k\\ \alpha_k\rho_k e_k\\ \alpha_k\end{bmatrix}, \quad G(Q_k) = \begin{bmatrix}\alpha_k\rho_k Y_k^i\boldsymbol{u}_k\\ \alpha_k\rho_k\boldsymbol{u}_k\otimes\boldsymbol{u}_k + \alpha_k p_k\\ \alpha_k(\rho_k e_k + p_k)\boldsymbol{u}_k\\ 0\end{bmatrix}, \quad H_k\cdot\nabla\alpha_k = \begin{bmatrix}0\\ p_I\nabla\alpha_k\\ p_I\boldsymbol{u_I}\cdot\nabla\alpha_k\\ -\boldsymbol{u_I}\cdot\nabla\alpha_k\end{bmatrix} \quad (5)$$

On the other hand, the source term writes:

$$R_k = \begin{bmatrix}w_k^i\\ \lambda(\boldsymbol{u_{k'}} - \boldsymbol{u_k}) + \boldsymbol{u_I}\nu(g_{k'} - g_k)\\ \boldsymbol{u_I}\cdot(\boldsymbol{u_{k'}} - \boldsymbol{u_k}) + p_I\mu(p_{k'} - p_k) + \theta(T_{k'} - T_k) + (\varepsilon_I + \boldsymbol{u_I}^2/2)\nu(g_{k'} - g_k)\\ -\mu(p_{k'} - p_k) + \theta(T_{k'} - T_k)/\kappa + \nu(g_{k'} - g_k)/\varrho\end{bmatrix} \quad (6)$$

2.2 The five equation model

The 7 equation model contains relaxation parameters λ and μ which determine the rates at which velocities and pressures of the phases reach equilibrium. Here we are interested in situations where relaxation times are small compared with the other physical characteristic times. From an asymptotic analysis, one can derive a 5 equation reduced model [39] including one equation for the volume fraction and one for the total mixture energy. This $(3+n_1+n_2)$ equation system extended here to the multi-species case will be referred to as the ‘‘(e,α) formulation’’.

$$\frac{\partial(\alpha_k\rho_k Y_k^i)}{\partial t} + div(\alpha_k\rho_k Y_k^i\boldsymbol{u}) = 0$$
$$\frac{\partial(\rho\boldsymbol{u})}{\partial t} + div(\rho\boldsymbol{u}\otimes\boldsymbol{u}) + \nabla p = 0$$
$$\frac{\partial(\rho e)}{\partial t} + div\big((\rho e + p)\boldsymbol{u}\big) = 0$$
$$\frac{\partial\alpha_2}{\partial t} + \boldsymbol{u}\cdot\nabla\alpha_2 = \alpha_1\alpha_2\frac{\rho_1 a_1^2 - \rho_2 a_2^2}{\alpha_1\rho_2 a_2^2 + \alpha_2\rho_1 a_1^2}div(\boldsymbol{u}) \quad (7)$$

DOI: 10.13009/EUCASS2017-147

Now, we establish a formulation of reduced model using two equations of transport for the internal energies instead of an equation for the volume fraction and another for the total mixture energy. If the different formulations are equivalent for smooth solutions, we expect the second one to be adapted for non-conservative terms as we will see in the next section 3. This second formulation of the 5 equation system will be referred to as the ''(ε_1,ε_2) formulation''. Thus we set $\lambda = \lambda_0/\varepsilon$ and $\mu = \mu_0/\varepsilon$ where ε tends to zero and we look for limit equations of the 7 equation model. In this way, we use an asymptotic expansion in terms of ε and we try to establish the governing equations when $\varepsilon \to 0$. This analysis can be performed directly on the conservative form of the system. However it is more convenient to work with the set of variables $(\alpha_k\rho_k, \boldsymbol{u}_k, \varepsilon_k, p_k, \alpha_k)$ and to use the quasi-linear form of the equations as in the following. Using the notation $D_k/Dt = \partial_t + \boldsymbol{u}_k \cdot \boldsymbol{\nabla}$ for the material derivative, from the momentum and the mass conservation equations, it is easily seen that the velocities $\boldsymbol{u}_k$ obey:

$$\alpha_k\rho_k D_k/Dt(\boldsymbol{u}_k) + \nabla(\alpha_k p_k) = p_I \nabla\alpha_k + \lambda(\boldsymbol{u}_{k'} - \boldsymbol{u}_k) \quad (8)$$

From these last equations, we deduce the ones for the kinetic energy $\boldsymbol{u}_k^2/2$ of each phase:

$$\alpha_k\rho_k D_k/Dt((\boldsymbol{u}_k)^2/2) + \boldsymbol{u}_k \cdot \nabla(\alpha_k p_k) = p_I \boldsymbol{u}_k \cdot \nabla\alpha_k + \lambda \boldsymbol{u}_k \cdot (\boldsymbol{u}_{k'} - \boldsymbol{u}_k) \quad (9)$$

Then from the total energy equations, we get the equations for the specific internal energies:

$$\alpha_k\rho_k D_k/Dt(\varepsilon_k) + \alpha_k p_k div(\boldsymbol{u}_k) = p_I(\boldsymbol{u_I} - \boldsymbol{u}_k) \cdot \nabla\alpha_k + \mu p_I(p_{k'} - p_k) + \lambda(\boldsymbol{u_I} - \boldsymbol{u}_k) \cdot (\boldsymbol{u}_{k'} - \boldsymbol{u}_k) \quad (10)$$

Now, we suppose a binary law state $\varepsilon_k = \varepsilon_k(\rho_k, p_k)$ and introduce the coefficients χ_k, κ_k for the partial derivatives:

$$\chi_k = \left.\frac{\partial\varepsilon_k}{\partial\rho_k}\right|_{p_k}, \kappa_k = \left.\frac{\partial\varepsilon_k}{\partial p_k}\right|_{\rho_k} \quad (11)$$

After some calculations, the transport equations for the pressures write:

$$\alpha_k D_k/Dt(p_k) + \alpha_k C_k div(\boldsymbol{u}_k) = C_{kI}(\boldsymbol{u_I} - \boldsymbol{u}_k) \cdot \nabla\alpha_k + \mu C_{kI}(p_{k'} - p_k) + \lambda/(\kappa_k\rho_k)(\boldsymbol{u_I} - \boldsymbol{u}_k) \cdot (\boldsymbol{u}_{k'} - \boldsymbol{u}_k) \quad (12)$$

In these last equations, we have introduced the phasic sound speed and the acoustic impedance for each phase. Then, $a_{kI}C_{kI}$ stand for the same quantities evaluated at the interfaces:

$$a_k^2 = \left.\frac{\partial p_k}{\partial\rho_k}\right|_{s_k} = \frac{1}{\kappa_k}\left(\frac{p_k}{\rho_k^2} - \chi_k\right), \qquad a_{kI}^2 = \frac{1}{\kappa_k}\left(\frac{p_I}{\rho_k^2} - \chi_k\right), \qquad C_k = \rho_k a_k^2, \qquad C_{kI} = \rho_k a_{kI}^2 \quad (13)$$

Now, we perform the asymptotic analysis introducing the following expansion in term of ε for velocities and pressures but also for the other variables:

$$\boldsymbol{u}_k = \boldsymbol{u}^0 + \varepsilon\boldsymbol{u}_k^1, \qquad p_k = p^0 + \varepsilon p_k^1 \quad (14)$$

The total mass conservation equations at order 0 read:

$$\frac{\partial(\alpha_k^0\rho_k^0)}{\partial t} + div(\alpha_k^0\rho_k^0\boldsymbol{u}^0) = 0 \quad (15)$$

The equations for velocities at order 0 read:

$$\alpha_k^0\rho_k^0\left(\frac{\partial\boldsymbol{u}^0}{\partial t} + \boldsymbol{u}^0 \cdot \nabla\boldsymbol{u}^0\right) + \nabla(\alpha_k^0 p^0) = p^0\nabla\alpha_k^0 + \lambda^0(\boldsymbol{u}_{k'}^1 - \boldsymbol{u}_k^1) \quad (16)$$

Then we can deduce at the order 0 the equations for internal energies and pressures:

$$\alpha_k^0\rho_k^0\left(\frac{\partial\varepsilon_k^0}{\partial t} + \boldsymbol{u}^0 \cdot \nabla\varepsilon_k^0\right) + \alpha_k^0 p^0 div(\boldsymbol{u}^0) = \mu p^0(p_{k'}^1 - p_k^1) \quad (17)$$

$$\alpha_k^0\left(\frac{\partial p^0}{\partial t} + \boldsymbol{u}^0 \cdot \nabla p^0\right) + \alpha_k^0 C_k^0 div(\boldsymbol{u}^0) = \mu^0 C_k^0(p_{k'}^1 - p_k^1) \quad (18)$$

Then, combining the above equations, we can get the pressures fluctuations at the order 1:

$$\mu^0(p_2^1 - p_1^1) = \alpha_1^0\alpha_2^0\frac{C_1^0 - C_2^0}{\alpha_1^0 C_2^0 + \alpha_2^0 C_1^0}\, div(\boldsymbol{u}^0) \quad (19)$$

Now, if we use the equations at order 0 for mass and internal energies, and we introduce the expression of the pressure fluctuations, we get for example for phase 1:

$$\alpha_1^0\rho_1^0\left(\frac{\partial\varepsilon_1^0}{\partial t} + \boldsymbol{u}^0 \cdot \nabla\varepsilon_1^0\right) + \alpha_1^0 p^0 div(\boldsymbol{u}^0) = \alpha_1^0\alpha_2^0 p^0\frac{C_1^0 - C_2^0}{\alpha_1^0 C_2^0 + \alpha_2^0 C_1^0}\, div(\boldsymbol{u}^0) \quad (20)$$

DOI: 10.13009/EUCASS2017-147

After the same manipulations for phase 2, and also using the mass conservation, internal energy equations read:

$$\frac{\partial \alpha_1^0 \rho_1^0 \varepsilon_1^0}{\partial t} + div(\alpha_1^0 \rho_1^0 \varepsilon_1^0 \boldsymbol{u}^0) = p^0 \left(\frac{-\alpha_1^0 C_2^0}{\alpha_1^0 C_2^0 + \alpha_2^0 C_1^0} \right) div(\boldsymbol{u}^0) \quad (21)$$

$$\frac{\partial \alpha_2^0 \rho_2^0 \varepsilon_2^0}{\partial t} + div(\alpha_2^0 \rho_2^0 \varepsilon_2^0 \boldsymbol{u}^0) = p^0 \left(\frac{-\alpha_2^0 C_1^0}{\alpha_1^0 C_2^0 + \alpha_2^0 C_1^0} \right) div(\boldsymbol{u}^0) \quad (22)$$

We point out that the mixture energy equation can be obtained by summing the two last equations and matches with the classical energy equation of ‘‘(e,α) formulation’’.

$$\partial_t(\rho^0 \varepsilon^0) + div(\rho^0 \varepsilon^0 \boldsymbol{u}^0) = -p^0 div(\boldsymbol{u}^0) \quad (23)$$

Finally, the 5 equation model referred to as the ‘‘(ε_1,ε_2) formulation’’ can be written under the form below. This new formulation will be used for the design of numerical fluxes in the next section 3.

$$\frac{\partial \left(\alpha_k \rho_k Y_k^i\right)}{\partial t} + div\left(\alpha_k \rho_k Y_k^i \boldsymbol{u}\right) = 0$$

$$\frac{\partial (\rho \boldsymbol{u})}{\partial t} + div(\rho \boldsymbol{u} \otimes \boldsymbol{u}) + \nabla p = 0$$

$$\frac{\partial \alpha_1 \rho_1 \varepsilon_1}{\partial t} + div(\alpha_1 \rho_1 \varepsilon_1 \boldsymbol{u}) = p \left(\frac{-\alpha_1 \rho_2 a_2^2}{\alpha_1 \rho_2 a_2^2 + \alpha_2 \rho_1 a_1^2} \right) div(\boldsymbol{u})$$

$$\frac{\partial \alpha_2 \rho_2 \varepsilon_2}{\partial t} + div(\alpha_2 \rho_2 \varepsilon_2 \boldsymbol{u}) = p \left(\frac{-\alpha_2 \rho_1 a_1^2}{\alpha_1 \rho_2 a_2^2 + \alpha_2 \rho_1 a_1^2} \right) div(\boldsymbol{u}) \quad (24)$$

3. Numerics

In this section, we propose for the 7 and 5 equation models several numerical upwind schemes in order to resolve the systems in a Finite Volume framework. A lot of works have been recently dedicated to liquid-gas interface problems. These types of two-phase flows exhibit strong gradients of variables and large variation of sound speed near the interface between the phases. In this context, it is mandatory to derive accurate but also very robust schemes. The class of upwind schemes based on the resolution of the Riemann problem seems to be a good candidate. For example in [15], a five equation reduced model is used with a HLLC scheme. Then in [34], a “new” 6 equation (2 pressures) hyperbolic model is proposed with a HLLC scheme and a low Mach preconditioning technique. In [49], [46], the same 6 equation is used with an acoustic and a HLLC solver. In [60], the 6 and 7 equation models with mechanical and thermal relaxations are solved by HLLC schemes.

For the 7 equation model, among the class of upwind schemes, we compare a VFRoe-ncv scheme [9], [4], [58] and the HLLC scheme [23]. The VFRoe schemes are based on the exact resolution of a linearized Riemann problem formulated in conservative variables or in any other independent system of variables. But as it will be presented in the following, these schemes suffer from a lack of robustness. As a consequence, we propose to study different HLLC type schemes based on the approximated solution of the non-linear Riemann problem. They seem to provide a maximum of robustness and accuracy. In the recent past a lot of works have been dedicated to apply the class of HLL [27], HLLC [50] upwind schemes on two-phase flow models. First of all, the HLL scheme has been applied to the 7 equation model in [48]. This scheme is very efficient for implementation but it suffers from a lack of accuracy. Then the work of [47] has proposed to restore contact discontinuities but the scheme is based on the assumption that the pressure and the velocity are instantaneously relaxed towards equilibrium. In [51], another HLLC type scheme has been derived but it is only valid for the interfacial pressure $p_I = p_1$ and velocity $\boldsymbol{u_I} = \boldsymbol{u}_2$ values of the original Baer-Nunziato 7 equation model [10]. Moreover, the scheme necessitates an iterative procedure to compute the intermediate states of the Riemann problem. In [2], a new scheme is proposed. It takes into account for the interfacial contact between fluids $\boldsymbol{u_I}$ but not for the two phasic contact discontinuities $\boldsymbol{u}_1, \boldsymbol{u}_2$. Finally, in [23], a HLLC involving all the waves of the Riemann problem is proposed. Among all these schemes, we have selected this one because it seems to be quite general and also adapted to restore a differential velocity between the two phases.

For the 5 equation model, we have presented two formulations of the system. The first one is the ‘‘(e,α) formulation’’ and the one second is the ‘‘(ε_1,ε_2) formulation’’. We propose to build HLLC type schemes based on these two formulations. The last one is very interesting and gives us the possibility to examine the most adapted closure of non-conservative terms satisfying total energy conservation. These shock computational difficulties due to non-conservative character of the model has to be examined carefully. This could help us to maintain positivity for crucial variables such as density, pressure or volume fraction.

DOI: 10.13009/EUCASS2017-147

Then an extension of the multi-slope technique [35] for this two-phase flow models and their specific variables has been implemented. When we are interested in two-phase flows, we have to deal with high density ratios, strong gradients and also discontinuous solutions. Nowadays, the MUSCL technique remains a good compromise between accuracy and robustness. For this reason, we have chosen the multi-slope approach for general unstructured meshes. As in the original MUSCL method, both a backward and a forward scalar slopes, are computed for each face of a given element.

3.1 VFRoe-ncv and HLLC schemes for the 7 equation model

The first scheme which has implemented for the 7 equation model is a VFRoe-ncv [9] formulated into entropic variables for sake of robustness. The principal ingredient of this scheme is to solve exactly a linearized Riemann problem. Details for this scheme can be found in [58]. As illustrated in the left of Figure 3, the Riemann problem is complex and involves 7 waves: $S_{L,k}, S_{M,k}, S_{R,k}, S_I$. The analysis of the Riemann problem shows that the characteristic fields associated to $S_{L,k}, S_{R,k}$ are genuinely nonlinear while fields associated to $S_{M,k}, S_I$ are linearly degenerate. Based on this mathematical structure, a VFRoe scheme in primitive variables has been proposed in [4]. In this paper, we choose a VFRoe-ncv scheme formulated in entropic variables to reach the maximum of robustness. Actually, using entropy equations allows us to satisfy a maximum principle on these variables when computing the solution of Riemann problem. The computation details of the diagonalization of the Jacobian matrix into entropic variables can be found in [58].

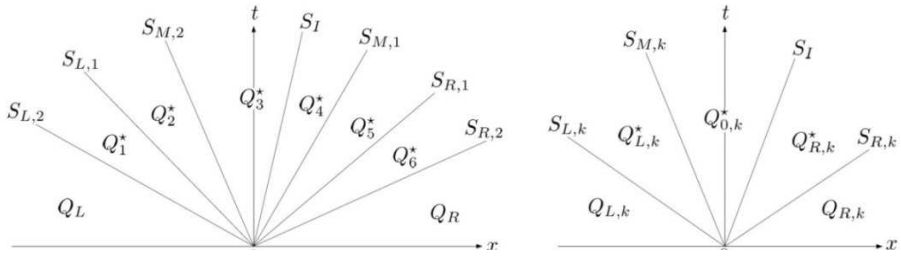

Figure 3: representation of the Riemann problem for the 7 equation model

Now, we describe the HLLC scheme for the 7 equation model. The non-conservative terms are decomposed into a conservative part and another one. Following the finite volume method and integrating the system on cell gives us:

$$V\frac{\partial Q_k}{\partial t} = \sum\left(-\boldsymbol{F}_{k,i}\cdot S_i\right) - \iiint \alpha_k \cdot \nabla \boldsymbol{H}_k dV \quad (25)$$

The expressions of the conservative and non-conservative parts of the semi-discretized system are given by:

$$\boldsymbol{F}_{k,i} = \begin{bmatrix} \alpha_k\rho_k Y_k^i u_{n,k} \\ \alpha_k\rho_k \boldsymbol{u}_k u_{n,k} + \alpha_k(p_k - p_I)\boldsymbol{n} \\ \alpha_k(\rho_k e_k + p_k)u_{n,k} - \alpha_k p_I u_{In} \\ \alpha_k u_{In} \end{bmatrix}, \quad \alpha_k \cdot \nabla H_k = \begin{bmatrix} 0 \\ \alpha_k \nabla p_I \\ \alpha_k div(p_I \boldsymbol{u_I}) \\ -\alpha_k div(\boldsymbol{u_I}) \end{bmatrix} \quad (26)$$

Then the integration is approximated with formula (27) where α_k is kept constant and evaluated at the center of the cell regarding the non-conservative term. Then, the evaluation of flux terms $\boldsymbol{F}_{k,i}, \boldsymbol{H}_{k,i}$ are performed by the HLLC solver which is briefly described in the sequel.

$$V\frac{\partial Q_k}{\partial t} = \sum\left(-\boldsymbol{F}_{k,i}\cdot S_i\right) - \alpha_k \cdot \sum\left(-\boldsymbol{H}_{k,i}\cdot S_i\right) \quad (27)$$

In [23], the conservative part of the flux $\boldsymbol{F}_{k,i}$ is computed with a quasi-classical monophasic HLLC for the phase *k*. Actually, the two principal assumptions of the scheme are a local constancy of interfacial velocity and pressure $\boldsymbol{u_I}, p_I$ and a local freezing of the volume fraction α inferring that α is supposed to vary only across the wave S_I.Thus, two consequences result from that. Firstly, we get a local conservative form of the Riemann problem because $\boldsymbol{u_I}, p_I$ are constant and there is no difficulty to express the different terms in a conservative form. Secondly, as illustrated in the right of Figure 3, we get two independent Riemann problems with four waves. Then to design the HLLC scheme, we need an important ingredient which is the evaluation of velocity of the waves:

$$S_{L,k} = min\left(u_{L,k} - a_{L,k}, u_{R,k} - a_{R,k}\right) \quad (28)$$

$$S_{R,k} = max\left(u_{L,k} + a_{L,k}, u_{R,k} + a_{R,k}\right) \quad (29)$$

$$S_{M,k} = \frac{\alpha_{R,k}(\rho u^2 + p)_{R,k} - \alpha_{L,k}(\rho u^2 + p)_{L,k} + S_{L,k}(\alpha\rho u)_{L,k} - S_{R,k}(\alpha\rho u)_{R,k} + \left(\alpha_{L,k} - \alpha_{R,k}\right)p_I}{(\alpha\rho u)_{R,k} - (\alpha\rho u)_{L,k} + S_{L,k}(\alpha\rho)_{L,k} - S_{R,k}(\alpha\rho)_{R,k}} \quad (30)$$

DOI: 10.13009/EUCASS2017-147

Moreover, we need to find the values of u_I and p_I in the star region. Inspired by the DEM [3], the interfacial velocity and pressure read respectively (31) and (32) for $\alpha_{1,L} < \alpha_{1,R}$ and $\alpha_{1,L} > \alpha_{1,R}$:

$$u_I = \frac{(\rho u^2 + p)_{R,1} - (\rho u^2 + p)_{L,2} + S_{L,2}(\rho u)_{L,2} - S_{R,1}(\rho u)_{R,1}}{(\rho u)_{R,1} - (\rho u)_{L,2} + S_{L,2}\rho_{L,2} - S_{R,1}\rho_{R,1}}, \quad p_I = \rho_{R,1}(u_{R,1} - S_{R,1})(u_{R,1} - u_I) + p_{R,1} \quad (31)$$

$$u_I = \frac{(\rho u^2 + p)_{R,2} - (\rho u^2 + p)_{L,1} + S_{L,1}(\rho u)_{L,1} - S_{R,2}(\rho u)_{R,2}}{(\rho u)_{R,2} - (\rho u)_{L,1} + S_{L,1}\rho_{L,1} - S_{R,2}\rho_{R,2}}, \quad p_I = \rho_{R,2}(u_{R,2} - S_{R,2})(u_{R,2} - u_I) + p_{R,2} \quad (32)$$

Then, the final expression for the HLLC flux can be written:

$$\begin{aligned} F^*_{L,K} &= F_{L,k} + S_{L,k}(Q^*_{L,K} - Q_{L,k}) \\ F^*_{0,K} &= F^*_{L,K} + S_A(Q^*_{0,K} - Q^*_{L,K}), \quad S_A = min(S_{M,k}, S_I) \\ F^*_{R,K} &= F^*_{0,K} + S_B(Q^*_{R,K} - Q^*_{0,K}), \quad S_B = max(S_{M,k}, S_I) \\ F_{R,k} &= F^*_{R,K} + S_{R,k}(Q_{R,k} - Q^*_{R,K}) \end{aligned} \quad (33)$$

3.2 HLLC type schemes for the 5 equation model

The different formulations of the 5 equation model derived in the previous section are used to build HLLC type schemes. The first step consists into writing the integration of the system on a cell using a Finite Volume approach.

$$V\frac{\partial Q}{\partial t} = \sum(-\boldsymbol{F}_i \cdot S_i) - \iiint \boldsymbol{K} div(\boldsymbol{u}) dV \quad (34)$$

The conservative part of the flux read respectively for the ''(e,α)" and the ''(ε_1,ε_2) formulations:

$$\boldsymbol{F}_i \cdot S_i = \begin{bmatrix} \alpha_k \rho_k Y^i_k u_n \\ \rho \boldsymbol{u} u_n + p\boldsymbol{n} \\ (\rho e + p) u_n \\ \alpha_2 u_n \end{bmatrix}, \quad \boldsymbol{F}_i \cdot S_i = \begin{bmatrix} \alpha_k \rho_k Y^i_k u_n \\ \rho \boldsymbol{u} u_n + p\boldsymbol{n} \\ \alpha_1 \rho_1 \varepsilon_1 u_n \\ \alpha_2 \rho_2 \varepsilon_2 u_n \end{bmatrix} \quad (35)$$

On the other hand, the non-conservative terms are given by the following expressions:

$$\boldsymbol{K} = \begin{bmatrix} 0 \\ 0 \\ 0 \\ -(\alpha_1 C_2)/(\alpha_2 C_1 + \alpha_1 C_2) \end{bmatrix}, \qquad \boldsymbol{K} = \begin{bmatrix} 0 \\ 0 \\ p(\alpha_1 C_2)/(\alpha_2 C_1 + \alpha_1 C_2) \\ p(\alpha_2 C_1)/(\alpha_2 C_1 + \alpha_1 C_2) \end{bmatrix} \quad (36)$$

If we consider the vector $\boldsymbol{K}$ constant in the cell, we can proceed to integration;

$$V\frac{\partial Q}{\partial t} = \sum -(\boldsymbol{F}_i + \boldsymbol{K} u_{n,i}) \cdot S_i \quad (37)$$

Then the conservative part of the flux at the interface is evaluated following the HLLC scheme described below. The wave velocities S_L, S_R, S_M are computed in a classical way and the intermediate states Q^*_L, Q^*_R in the star region read:

$$\frac{u_{n,L} - S_L}{S_M - S_L}\begin{pmatrix} \alpha_{k,L}\rho_{k,L}Y^i_{k,L} \\ \rho_L[\boldsymbol{u}_L + (S_M - u_{n,L})\boldsymbol{n}] \\ \rho_L\left[e_L + \frac{p_L}{\rho_L}\frac{u_{n,L} - S_M}{u_{n,L} - S_L} + (S_M - u_{n,L})S_M\right] \end{pmatrix}, \frac{u_{n,R} - S_R}{S_M - S_R}\begin{pmatrix} \alpha_{k,R}\rho_{k,R}Y^i_{k,R} \\ \rho_R[\boldsymbol{u}_R + (S_M - u_{n,R})\boldsymbol{n}] \\ \rho_R\left[e_R + \frac{p_R}{\rho_R}\frac{u_{n,R} - S_M}{u_{n,R} - S_R} + (S_M - u_{n,R})S_M\right] \end{pmatrix} \quad (38)$$

Then the HLLC flux can be written under the form:

$$\begin{aligned} F = \frac{F_L + F_R}{2} + \frac{\sigma_L + \sigma_R}{2}\frac{F_L - F_R}{2} + \frac{\sigma_R - \sigma_L}{2}\left[\frac{S_L}{2}(Q^*_L - Q_L) + \frac{S_R}{2}(Q^*_R - Q_R) + \sigma_M\frac{S_M}{2}(Q^*_L - Q^*_R)\right] \\ \sigma_L = sign(S_L), \qquad \sigma_R = sign(S_R), \qquad \sigma_M = sign(S_M) \end{aligned} \quad (39)$$

For non-conservative terms, the same method as in [49] for a 6 equation (two pressures) model is used. It consists to use the solution of the Riemann problem. First, we consider the ''(e,α) formulation'' of the model and the only one non conservative equation for the volume fraction writes:

$$V\frac{\partial \alpha_1}{\partial t} = \sum -\left[(\widehat{\alpha_1 u_n})_i + \boldsymbol{K}\hat{u}_{n,i}\right]S_i \quad (40)$$

Then, according to the sign of the waves S_L, S_R, S_M, we are able to compute:

$$(\widehat{\alpha_1 u_n})_i = (\alpha_{1,L}u_{n,L}, \alpha^*_{1,L}S_M, \alpha^*_{1,R}S_M, \alpha_{1,R}u_R), \quad \hat{u}_{n,i} = (u_{n,L}, S_M, S_M, u_R) \quad (41)$$

DOI: 10.13009/EUCASS2017-147

Then combining, the two components of the mass fractions (38) in the star region, the volume fractions read:

$$\alpha_{1,L}^{*}=\frac{R_L}{1+R_L},\qquad R_L=\frac{(\alpha_1\rho_1)_L}{(\alpha_2\rho_2)_L}\frac{\rho_{2,L}^{*}}{\rho_{1,L}^{*}},\quad \alpha_{1,R}^{*}=\frac{R_R}{1+R_R},\qquad R_L=\frac{(\alpha_1\rho_1)_R}{(\alpha_2\rho_2)_R}\frac{\rho_{2,R}^{*}}{\rho_{1,R}^{*}}\quad (42)$$

Then, let us suppose isentropic rarefaction across the waves S_L , S_R and we can deduce the real phasic density:

$$\rho_{k,L}^{*}-\rho_{k,L}=\frac{p_L^{*}-p_L}{\hat{a}_{k,L}^{2}},\quad \rho_{k,R}^{*}-\rho_{k,R}=\frac{p_R^{*}-p_R}{\hat{a}_{k,R}^{2}}\quad (43)$$

Now, we consider the second ''(ε_1,ε_2) formulation'' of the 5 equation model. We have to deal with the non-conservative equations for the internal energy of each phase:

$$V\frac{\partial\alpha_k\rho_k\varepsilon_k}{\partial t}=\sum\left[-(\alpha_k\widehat{\rho_k\varepsilon_k}u_n)_i+\boldsymbol{K}\hat{u}_{n,i}\right]S_i\quad (44)$$

Then, according to the sign of the waves S_L , S_R, S_M , we are able to compute:

$$(\alpha_k\widehat{\rho_k\varepsilon_k}u_n)_i=\left((\alpha_k\rho_k)_L\varepsilon_{k,L}u_L,(\alpha_k\rho_k)_L^{*}\varepsilon_{k,L}^{*}S_M,(\alpha_k\rho_k)_R^{*}\varepsilon_{k,R}^{*}S_M,(\alpha_k\rho_k)_R\varepsilon_{k,R}u_R\right),\ \ \hat{u}_{n,i}=\left(u_{n,L},S_M,S_M,u_R\right)\quad (45)$$

Now we have to determine the values of internal energies in the star region $\varepsilon_{k,L}^{*},\varepsilon_{k,R}^{*}$ which are the only unknowns. We have implemented and tested different solutions.

$$\varepsilon_{k,L}^{*}=\varepsilon_{k,L}\quad option\ (a)\quad (46)$$

$$\varepsilon_{k,L}^{*}=\varepsilon\left(\rho_{k,L}^{*},p^{*}\right)\quad option\ (b)\quad (47)$$

$$T_{k,L}^{*}=T_{k,L},\varepsilon_{k,L}^{*}=\varepsilon\left(T_{k,L}^{*},p^{*}\right)\quad option\ (c)\quad (48)$$

Then the option (d) is based on a close examination of the jump relation for energy:

$$(\alpha_k\rho_k)_L^{*}(u^{*}-S_L)=\alpha_k\rho_k(u-S_L),p^{*}=p+\rho(u-S_L)(u-u^{*}),\rho^{*}e^{*}(u^{*}-S_L)=\ \rho e(u-S_L)-p^{*}u^{*}+pu\ (49)$$

Then let us introduce the specific volume $v=1/\rho$ and write the jump relations for internal energy:

$$u^{*}-u=m(v^{*}-v),\quad p^{*}-p=m^{2}(v^{*}-v)$$

$$m(\varepsilon^{*}-\varepsilon)=mu^{2}/2-m(u^{*})^{2}/2-p^{*}u^{*}+pu,\ \ \varepsilon^{*}-\varepsilon=(p+p^{*})(v-v^{*})/2\quad (50)$$

As non-conservative terms are not adapted for the determination of the jump, we propose to use mixture energy:

$$\varepsilon_k^{*}-\varepsilon_k=(p_k+p_k^{*})(v_k-v_k^{*})/2,\ \ \varepsilon^{*}=\varepsilon+(p+p^{*})(\alpha_2v-\alpha_2^{*}v^{*}+\alpha_1v-\alpha_1^{*}v^{*})/2\quad (51)$$

The last equality is obtained thanks to the relation $Y_k = Y_k^{*}$. But, there is a problem to find v_k^{*} because α_1 varies across S_L , S_R. So the following approximation is made:

$$\varepsilon_k^{*}-\varepsilon_k=(p+p^{*})(v-v^{*})/2\quad option\ (d)\quad (52)$$

Finally, the option (e) is based on a correction for the mixture energy for conservation:

$$\varepsilon_k^{*}-\varepsilon_k=p(\rho_k^{*}-\rho_k)/\rho_k^{2},\quad \rho_{k,L}^{*}-\rho_{k,L}=(p_L^{*}-p_L)/\hat{a}_{k,L}^{2}$$

$$(\alpha_k\rho_k\varepsilon_k)^{corrected}=\alpha_k\rho_k\varepsilon_k+K_k\Delta(\rho\varepsilon),\qquad K_1+K_2=1\ option\ (e)\quad (53)$$

4. Results

In this section, we present the numerical results obtained with the diffuse interface model using HLLC schemes combined with the specific MUSCL technique [35]. The first part of the test deals with classical shock tube. The second part of the test handles with two-phase flow problems including interface liquid gas instabilities and a coaxial injector configuration based on MASCOTTE test bench [53].

4.1 Results obtained with the 7 equation model

4.1.1 Two-phase flow shock tube

For this first test case, VFRoe-ncv [58] and HLLC [23], [6] schemes have been able to perform. The Stiffened Gas equation of state [33] has been used and takes into account for attractive and repulsive effects.

$$p_k=(\gamma_k-1)\rho_k(\varepsilon_k-q_k)-\gamma_k\pi_k=(\gamma_k-1)c_{vk}T_k-\pi_k\quad (54)$$

$$\varepsilon_k=c_{vk}T_k+\pi_k/\rho_k\quad (55)$$

DOI: 10.13009/EUCASS2017-147

The Stiffened Gas law is used for both gas and liquid. Parameters are summarized below for the air and the water:

$$\gamma_k = 1.4, \quad c_{vk} = 1000, \quad \pi_k = 0$$
$$\gamma_k = 4.4, \quad c_{vk} = 4000, \quad \pi_k = 6.10^8 \quad (56)$$

This is a classical shock tube where the two phases are simultaneously present at the same location. The volume fraction is constant and equal to $\alpha = 0.5$ everywhere in the domain. The water with density $\rho_2 = 1000$ kg/m^3 is located on the left side and the air with $\rho_1 = 50$ kg/m^3 is on the right side. On the left side ($x < 0.5$) the pressure is equal to 10^9 Pa while it is equal to 10^5 Pa on the right side. The velocity is zero at time 0. The discretization is done on a 1000 cells grid and the CFL number equal to 0.0005n with n the iterations number and then fixed to 0.5. The results are shown at time 200µs. We compare the results obtained with VFRoe-ncv and HLLC schemes. The Figure 4 plots the evolution of the relaxed pressure and velocity. Then Figure 4 plots also the volume fraction, the density, the temperature and the monophasic variable $\alpha_k\rho_k$ for each phase. Finally, we observe that even if the initial composition of the mixture is constant, it evolves in space and time because of mechanical effects due to pressure relaxation. The second order in space is obtained with the MUSCL technique [35]. The time integration is based on a classical second order, two stages TVD Runge–Kutta scheme. The results for VFRoe-ncv and HLLC schemes are equivalent in term of accuracy and allow us to validate the implementation of the HLLC scheme for the 7 equation model.

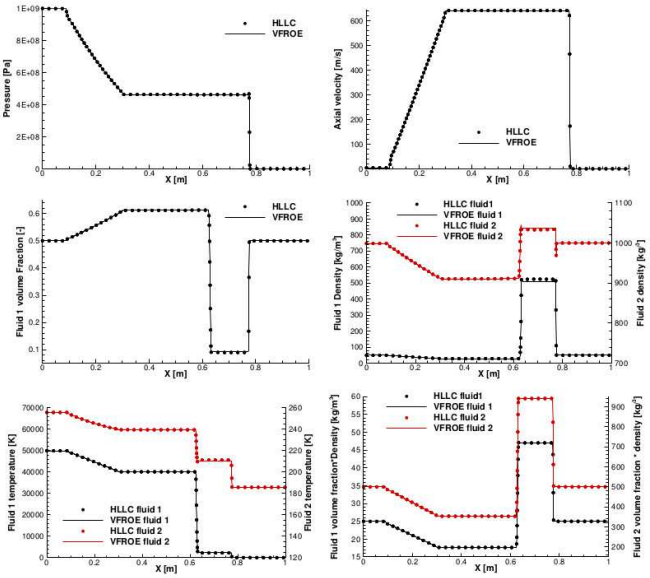

Figure 4: two-phase flow shock tube with the 7 equation model (comparison between VFRoe and HLLC schemes)

4.1.2 Shear layer instabilities test case

Here we present a shear layer test case which is representative of liquid gas interface instabilities occurring in the coaxial injector configuration. As depicted in Figure 5, the box is 2m large and 1m high and the size mesh is equal to 4mm. We point out that an important parameter of the flow is the difference velocity between the two phases.

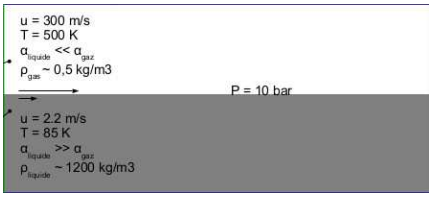

Figure 5: shear layer test case geometry

The Stiffened Gas law is used for both gas and liquid. The parameters have been chosen in order to reach a density of 1200 kg/m^3 for a temperature of 85K and a pressure of 10 bars for the liquid oxygen. In the same way, the density is equal to 0.86 kg/m3 for a temperature of 280K and a pressure of 10 bars for the gaseous hydrogen. These conditions match with the injection of MASCOTTE facility at the 10 bar point. The Stiffened-Gas EOS parameters for LOx and GH_2 parameters are summarized below:

$$\gamma_k = 1.41, \quad c_{vk} = 10112, \quad \pi_k = 7.173.10^7$$
$$\gamma_k = 1.77, \quad c_{vk} = 951, \quad \pi_k = 0 \quad (57)$$

DOI: 10.13009/EUCASS2017-147

For the VFRoe-ncv scheme, the largest differential of velocities which has been possible to compute is equal to 300-100 m/s. The top and bottom parts of the box contain nearly pure fluids. The volume fraction of the gas in the liquid part is equal to ε=0.01 and inversely in the liquid part. We point out that this residual value fixed to ε=0.01 is too high but it hasn't been possible to decrease this value because of robustness. The infinite relaxation velocity has to be used. The time step has been evaluated with a CFL=0.1. For the VFRoe-ncv, there is a real problem of robustness when we consider the simulation of interface liqud-gas instabilities. So, the necessity of a more robust scheme seems to be clear if we want to deal with largest difference velocity between the two phases. Only the HLLC scheme has been able to compute this configuration of shear layer with a large differential velocity of 300-2 m/s. Computations have been perform with and without infinite relaxation velocity. The interface is much more destabilized with relaxation as illustrated in Figure 6 plotting the volume fraction fields. The residual value of ε in the nearly pure fluids is equal to $\varepsilon=10^{-3}$ and the initial velocity of the liquid is equal to 2 m/s. The MUSCL technique has been also used to reach second order space accuracy. The classical Van Leer limitation has been used for MUSCL technique.

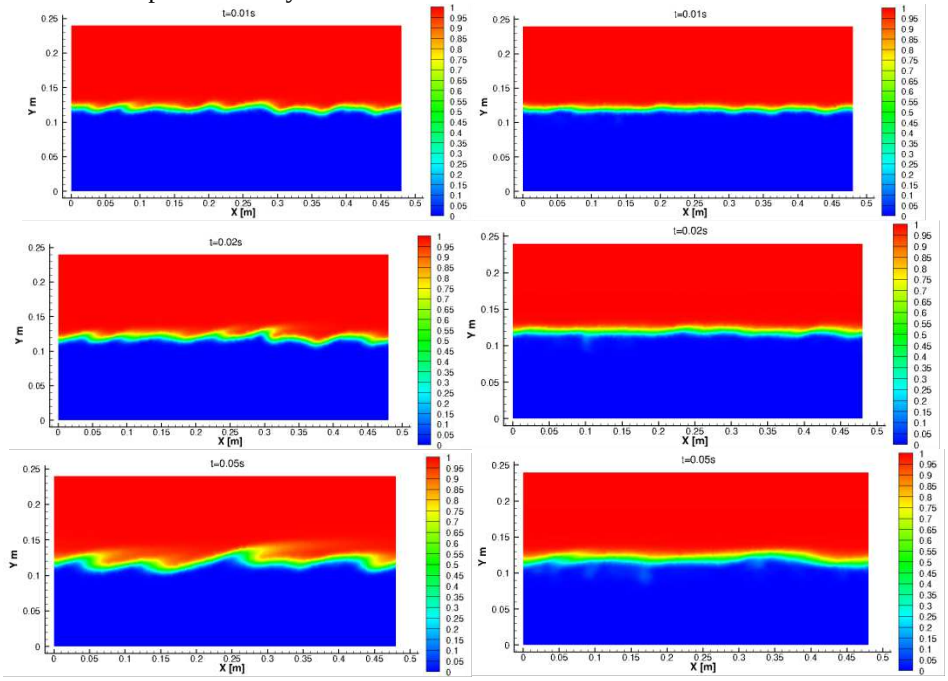

Figure 6: results for the volume fraction field obtained with the 7 equation model on the shear layer test case with infinite relaxation velocities (left) and without velocity relaxation (right)

4.1.3 Coaxial injector (2D configuration)

In this las test case, we propose a two dimensional configuration of a coaxial cryogenic injector based on the MASCOTTE [53] facility as depicted in Figure 7. The same fluids and parameters of the Stiffened gas law state than previously for the shear layer have been used. The residual value of ε is equal to $\varepsilon=10^{-6}$. To restore the interfacial transfer of momentum velocities, we don't use infinite procedure relaxation of velocities in the region of the diffuse interface defined by $0.001<\alpha<0.999$ for the gas and $0.00001<\alpha<0.99999$ for the liquid. Results are presented in Figure 8 for a simulation during a physical time equal to 0.01s and seem to be very promising. Figure 9 plots the velocities of the two phases and show that the simulation is able to provide both the liquid and gas velocities. In a near future, we expect that restoring the differential velocity between the two phases and modelling the interfacial transfer could help us for the modelling of atomization.

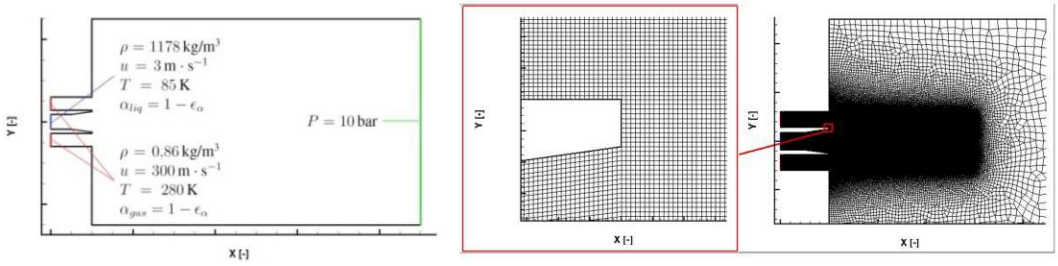

Figure 7: two dimensional configuration of a coaxial injector based on MASCOTTE test facility

DOI: 10.13009/EUCASS2017-147

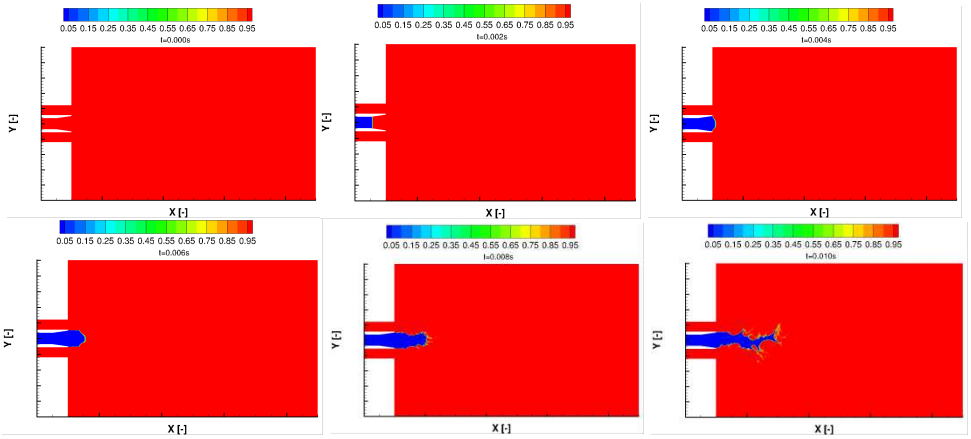

Figure 8: results for the volume fraction field obtained on the two dimensional configuration of a coaxial injector

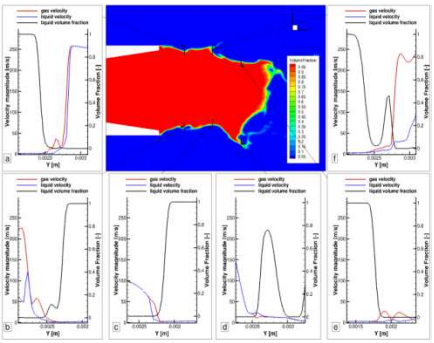

Figure 9: results for the LOx and GH_2 velocities obtained on the two dimensional configuration of a coaxial injector

4.2 Results obtained with the 5 equation model

4.2.1 Water-air shock tube

The length of the domain is 1 m and initially the interface is located at x = 0.7 m. The tube is initially filled with a high pressure liquid water and on the right side with air. This test problem consists of a classical shock tube with two fluids and admits an exact solution. The initial condition consists in a pressure discontinuity between $p = 10^9$ Pa in the liquid side and $p = 10^5$ Pa in the gas side. As in the previous test case, the right and left chambers contain nearly pure fluids: the volume fraction of the gas in the water chamber is 10^{-8} and inversely the water volume fraction is 10^{-8} in the gas chamber. This computation uses a mesh with 1000 cells, with a CFL number equal to CFL = max(0.001n,0.8) where n is the iteration number. Figure 10 displays for the different numerical methods the volume fraction, the mixture density, the pressure and the velocity. The exact solutions are represented on these curves. The results are shown at time 229µs and seem to be of comparable accuracy with respect to the exact solution. Figure 10 plots the results at the order 1 and 2 in space. For the monophasic variables such as the temperatures, we emphasize that different schemes could give very different results and could lead to very different level of robustness. Nevertheless, the formulation with two internal energies seems very promising compared to the one with the volume fraction and total energy transport equations.

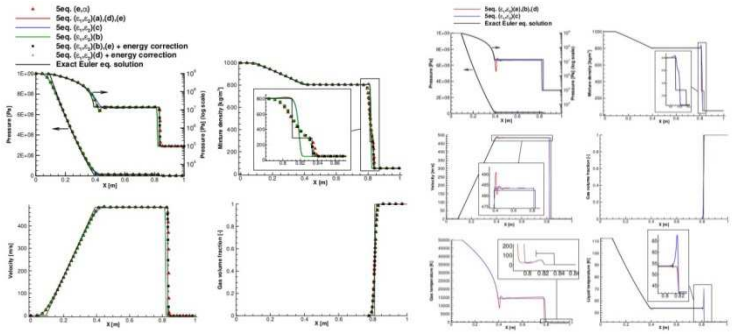

Figure 10: results of the 5 equation model on the water air shock tube at the order 1 and 2

DOI: 10.13009/EUCASS2017-147

4.2.2 Coaxial injector (3D configuration)

Finally, we present a cryogenic injector test case based on the MASCOTTE [53] test facility configuration. In order to reduce mesh size and solution time, the simulation is performed with a 60° sector geometry. The geometry, the mesh and an instantaneous iso-surface of the volume fraction are presented in Figure 11. Then, Figure 12 plots the instantaneous field for the volume fraction and the evolution of the pressure and temperature. The results seem very promising and we point out that there are no spurious oscillations for the pressure or the temperature neither for the gas nor for the liquid. The law state for the LOx taking into account for liquid compressibility reads:

$$\rho(T,p) = \frac{1}{v} = \frac{1}{v_0}\frac{1+\beta_0(P-P_0)}{1+\alpha_0(T-T_0)} \quad (58)$$

The different parameters are summarized below:

$$P_0 = 10bar, T_0 = 85K, v_0 = 8{,}54.10^{-3}m^3/kg, \alpha_0 = 4.12\ 10^{-3}, \beta_0 = 1.71\ 10^{-9}, c_v = 951J/kg/K \quad (59)$$

On the other hand a classical "perfect" Stiffened gas law state is used for the GH_2:

$$\gamma = 1.4, \qquad \pi = 0, \qquad c_v = 10112J/kg/K \quad (60)$$

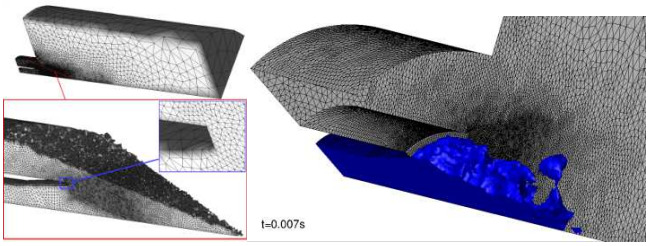

Figure 11: 3D geometry and mesh of the coaxial injector and result for an iso-surface the volume fraction

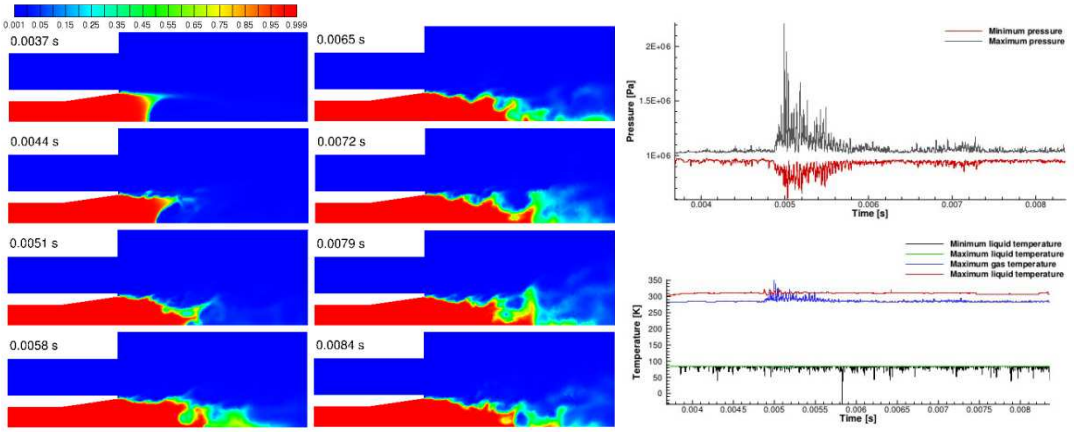

Figure 12: results obtained with the 5 equation model for the coaxial cryogenic injector (3D configuration)

5. Conclusion

In this paper, we have proposed interface diffuse models to deal with the "separated" two-phase flow in coaxial cryogenic injector. Firstly, we have proposed a 7 equation model with two pressures, velocities and temperatures. For this complex model, we have implemented an efficient HLLC scheme and applied to a coaxial cryogenic injector considering the inert case. Results obtained with the 7 equation model are very promising and we expect that restoring the differential of velocity between phases could help us when modelling the atomization. Secondly, we have proposed a 5 equation model which has a simple mathematical structure close to the 4 equation model excepted for non-conservative terms. To deal with these terms, we have derived a two internal energies formulation and proposed different HLLC type schemes. This model is able to restore the correct temperature of liquid and gas in the simulation. This will be very important in the reactive case configuration. This 5 equation model could represent a good alternative between the 4 and the 7 equation models. It could be completed by information for the liquid velocity. In a near future, we intend to couple these two models with a kinetic solver for the spray following the strategy of [40] in order to deal with atomization and combustion.

DOI: 10.13009/EUCASS2017-147

References

[1] A. Andreini, C. Bianchini, S. Puggelli, F.X. Demoulin (2016). Development of a turbulent liquid flux model for Eulerian-Eulerian multiphase flow simulations. *Intl Journal of Multiphase flow*. 81:88–103.

[2] A. Ambroso, C. Chalons, P. A. Raviart (2012). A Godunov-type method for the seven-equation model of compressible two-phase flow. *Computers & Fluids* 54:67–91.

[3] R. Abgrall, R. Saurel (2003). Discrete equations for physical and numerical compressible multiphase mixtures. *Journal of Computational Physics*. 186:361–396.

[4] N. Andrianov, G. Warnecke (2004). The RP for the BN two-phase flow model. JCP. 195:434–464

[5] P. A. Beau (2006). Modélisation de l'atomisation d'un jet liquide. Application aux sprays Diesel. Thèse de doctorat. Université de Rouen.

[6] A. Boucher (2015). Développement d'un modèle pour la simulation de l'atomisation dans les chambres de combustion des moteurs fusées à ergols liquides – Rapport d'activités 2015. RT 8/22894 DEFA.

[7] A. Boucher (2016). Développement d'un modèle pour la simulation de l'atomisation dans les chambres de combustion des moteurs fusées à ergols liquides – Rapport d'activités 2016. RT 11/22894 DEFA.

[8] Z. Bouali, B. Duret, F.X. Demoulin, A. Mura (2016). DNS analysis of small scal turbulence scalar interaction in evaporating two phase flows. *International Journal of Multiphase flow*. 85:326–335.

[9] T. Buffard, T. Gallouet, J.M. Herrard (2000). A sequel to a Rough Godunov Scheme: Application to Real Gases. *Computers and Fluids*. 29:673–709.

[10] M.R. Baer and J.W. Nunziato (1986). A two-phase mixture theory for the deflagration-to-detonation transition (DDT) in reactive granular materials. *Journal of Multiphase flows*. 12:861–889.

[11] J. Chesnel (2010). Simulation aux Grandes Échelles de l'Atomisation. Application à l'Injection Automobile. Thèse de doctorat. Université de Rouen.

[12] J. Chesnel, T. Menard, J. Reveillon, F.-X. Demoulin (2011). Subgrid analysis of liquid jet atomization. *Atomization and Sprays*. 21(1):41–67.

[13] J. Chesnel, J. Reveillon, T. Menard, F.-X. Demoulin (2011). Large eddy simulation of liquid jet atomization. *Atomization and Sprays*. 21(9):711–736.

[14] C. Crua, T. Shoba, M. Heikal, M. Gold, C. Higham (2010). High-speed microscopic imaging of the initial stage of diesel spray formation and primary breakup. SAE 2010–01–2247.

[15] A. Daramizadeh, M. R. Ansari (2015). Numerical simulation of underwater explosion near air–water free surface using a five-equation reduced model. Ocean Engineering. 110(Part A):25–35

[16] F.X. Demoulin, P.-A. Beau, G. Blokkeel, A. Mura, R. Borghi (2007). A new model for turbulent flows with large density fluctuations: application to liquid atomization. *Atomization & Sprays*. 17(4):315–345.

[17] B.M. Devassy, C. Habchi, E. Daniel (2015). Atomization modelling of liquid jets using a two-surface-density approach. *Atomization and Sprays*. 25(1):47–80.

[18] D.A. Drew, S.L. Passman (1998). Theory of multicomponent fluids. Applied Mathematical Sciences, vol. 135, Springer, New York.

[19] A. Desjardins, H. Pitsch (2010). Detailed numerical investigation of turbulent atomization of liquid jets. *Atomization Sprays*. 20(4):311–336.

[20] F.X. Demoulin, J. Reveillon, B. Duret, Z. Bouali, P. Desjonqueres, T. Menard (2013). Toward using direct numerical simulation to improve primary break-up modeling. *Atom and Sprays*. 23(11):957–980.

[21] B. Duret, J. Reveillon, T. Menard, F.X. Demoulin (2013). Improving primary atomization modeling through DNS of two-phase flows. *International Journal of Multiphase Flow*. 55:130–13.

[22] D. Fuster, A. Bague, T. Boeck, L. Le Moyne, A. Leboissetier, S. Popinet, P. Ray, R. Scardovelli, S. Zaleski (2009). Simulation of primary atomization with an octree adaptive mesh and VOF method, *IJMF*. (35)550–565.

[23] D. Furfaro, R. Saurel (2015). A simple HLLC-type Riemann solver for compressible non-equilibrium two-phase flows. *Computers and fluids*. 111:159–178.

[24] P. Gicquel, E. Porcheron, E. Brisson (1998). Caractérisation expérimentale en combustion d'un brouillard LOX-GH2 issu d'un injecteur coaxial (campagne d'essais 1997 à 1 MPa). ONERA RT 98/6128 DEFA/Y/DMTE.

[25] M. Herrmann (2010). A parallel Eulerian interface tracking/Lagrangian point particle multi-scale coupling procedure. *Journal of Computational Physics*. 229: 745–759.

[26] M. Herrmann (2011). On simulating primary atomization using the refines level set grid method, *Atomization and Sprays*. 21(4):283–301.

[27] A. Harten, P. Lax, B. Van Leer (1983). On Upstream Differencing and Godunov-Type Schemes for Hyperbolic Conservation Laws. SIAM Review. 25(1):35–61.

[28] M. Ishii (1975). Thermo-Fluid Dynamic Theory of Two-phase flow. Volume 22 of Direction des études et recherches d'électricité de France. Eyrolles, Paris.

[29] S. Jay (2003). Modélisation de la combustion diphasique au moyen de bilans d'aire interfaciale et de surface de flamme. Application à la combustion cryotechnique. Thèse de doctorat. Ecole Centrale Paris.

DOI: 10.13009/EUCASS2017-147

[30] S. Jay, F Lacas, S Candel (2006). Combined surface density concepts for dense spray combustion. Combustion and Flame. 144(3):558–577.
[31] R. Lebas (2007). Modélisation Eulérienne de l'Atomisation Haute Pression - Influences sur la Vaporisation et la Combustion Induite. Thèse de doctorat. Université de Rouen.
[32] R. Lebas, T. Menard, P.A. Beau, A. Berlemont, F.X. Demoulin (2009). Numerical simulation of primary break-up and atomization : DNS and modelling study. *Int Journal of Multiphase flow*. 35:247–260.
[33] O. Le Métayer, J. Massoni, R. Saurel (2004). Elaborating equations of state of a liquid and its vapor for two-phase flow model. International Journal of Thermal Sciences. 43:265–276.
[34] S. LeMartelot, B. NKonga, R. Saurel. (2013). Liquid and liquid-gas flows at all speeds. *Journal of Computational Physics*. 255:53–82.
[35] C. Le Touze, A. Murrone, H. Guillard (2015). Multislope MUSCL method for general unstructured meshes. *Journal of Computational Physics*. 284:389–418.
[36] N. Meyers, (2006). Modélisation de la combustion cryotechnique avec prise en compte de l'atomisation primaire du jet d'oxygène liquide. Thèse de doctorat. Université d'Aix-Marseille II.
[37] C. Morel (2007). On the surface equations in two phase flows and reacting single phase flows. *International Journal of Multiphase Flows*. 33(10): 1045–1073.
[38] A. Murrone, N. Fdida, C. Le Touze, L. Vingert (2014). Atomization of cryogenic rocket engines coaxial injectors. Modeling aspects and experimental investigations. In: Space Propulsion. Cologne, Germany.
[39] A. Murrone, H. Guillard (2005). A five equation reduced model for compressible two phase flow problems. *Journal of computational Physics*. 202:664–698.
[40] A. Murrone, C. Le Touze (2015). Eulerian coupling of two-phase flow models for the Large Eddy Simulation of the atomization in cryogenic combustion chamber. In: 6th EUCASS 2015.
[41] T. Menard, S. Tanguy, A. Berlement (2007). Coupling level set/vof ghost fluid methods: validation and application to 3d simulation of the primary breakup of a liquid jet. *IJMF*. 33(5):510–524.
[42] P. Marmottant, E. Villermaux (2004). On spray formation. *Journal of Fluid Mechanics*. 498:73–112.
[43] A. Murrone, P. Villedieu (2011). Numerical Modeling of Dispersed Two-Phase Flows. THE ONERA JOURNAL AerospaceLab, Issue 2, March 2011 - CFD Platforms and Coupling.
[44] A.R. Osta, J. Lee, K.A. Sallam, K. Fezzaa (2012). Study of the effects of the injector length/diameter ratio on the surface properties of turbulent liquid jets in still air using x-ray imaging. *IJMF*. (38):87–98.
[45] M. Pourouchottamane (2002). Modélisation des brouillards denses pour la combustion cryotechnique. Thèse de doctorat. Université d'Aix-Marseille II.
[46] M. Pelanti, K.M. Shyue (2014). A mixture-energy-consistent six-equation two phase numerical model for fluids with interfaces, cavitation and evaporation waves. *Journal of Computational Physics*. 259:331–357.
[47] L. Qiang, F. Jian-Hu, C. Ti-Min, H. Chun-Bo (2004). Difference scheme for two-phase flow. *Applied Mathematics and Mechanics*. 25(5):536–545.
[48] R. Saurel, R. Abgrall (1999). A Multiphase Godunov Method for Compressible Multifluid and Multiphase Flows. *Journal of Computational Physics*. 150:427–460.
[49] R. Saurel, F. Petitpas, Ray A. Berry. (2009). Simple and efficient relaxation method for interfaces separating compressible fluids, cavitating flows and shocks in multiphase mixtures. *JCP*. 228:1678–1712.
[50] E. F. Toro, M. Spruce, W. Speares (1994). Restoration of the contact surface in HLL solver. *SW*. 4(1):25–34.
[51] S. A. Tokareva, F. Toro (2010). HLLC-type Riemann solver for the Baer–Nunziato equations of compressible two-phase flow. *Journal of Computational Physics*. 229(10):3573–3604.
[52] A. Vallet (1997). Contribution à la Modélisation de l'Atomisation d'un Jet Liquide Haute Pression. Thèse de doct. Université de Rouen, 1997.
[53] L. Vingert (2006). Sélection de cas tests Mascotte : - cas subcritique LOX/GH2 10 bar. - cas supercritique LOX/GH2 60 bar. Rapport technique RT 1/11785. ONERA.
[54] C. Vessiller (2008). Contribution à l'étude des Bouillards Denses et Dilués par les Approches Eulériennes et Lagrangiennes, PhD Thesis, Ecole Centrale Paris, Paris, France.
[55] A. Vallet, R. Borghi (1999). Modélisation Eulérienne de l'atomisation d'un jet liquide, C.R. Acad. Sci. Paris Sér. II b, vol. 327(10):1015–1020.
[56] A. Vallet, A. Burluka and R. Borghi (2001). Development of an Eulerian model for the atomization of a liquid jet. *Atomization and Sprays*. 11:619–642.
[57] L. Vingert, M. Habiballah and J.C. Traineau (1999). MASCOTTE: a research facility for high pressure combustion of cryogenic propellants. In: 12th European Aerospace Conference, Paris.
[58] F. Vuillot, D. Zuzio, A. Murrone (2015). CEDRE, solveur multi-fluides: travaux 2014. RT 1/23121.
[59] Wang, X. Liu, K.S. Im, W.K. Lee, J. Wang, K. Fezzaa, D.L.S. Hung and J.R. Winkelman (2008). Ultrafast x-ray study of dense liquid jet flow dynamics using structure tracking velocimetry, Nat. Phys., 4:305–309.
[60] A. Zein, M. Hantke, G. Warnecke. (2010). Modeling phase transition for compressible two-phase flows applied to metastable liquids. *Journal of Computational Physics*. 229:2964–2998.